



# Measurement of chlorine concentration on steel surfaces via fiber-optic laser-induced breakdown spectroscopy in double-pulse configuration

X. Xiao<sup>a, b</sup>, S. Le Berre<sup>b</sup>, D.G. Fobar<sup>a</sup>, M. Burger<sup>a, d</sup>, P.J. Skrodzki<sup>a, d</sup>, K.C. Hartig<sup>b, c</sup>, A.T. Motta<sup>b</sup>, I. Jovanovic<sup>a, d, \*</sup>

<sup>a</sup> Department of Nuclear Engineering and Radiological Sciences, University of Michigan, Ann Arbor, MI 48109, United States

<sup>b</sup> Department of Mechanical and Nuclear Engineering, The Pennsylvania State University, University Park, PA 16802, United States

<sup>c</sup> Nuclear Engineering Program, University of Florida, Gainesville, FL 32611, United States

<sup>d</sup> Center for Ultrafast Optical Science, University of Michigan, Ann Arbor, MI 48109, United States

## ARTICLE INFO

### Article history:

Received 6 October 2017

Received in revised form 10 January 2018

Accepted 11 January 2018

Available online xxx

### Keywords:

Laser-induced breakdown spectroscopy (LIBS)  
Optical fiber  
Remote inspection  
Double pulse  
Chlorine

## ABSTRACT

The corrosive environment provided by chlorine ions on the welds of stainless steel dry cask storage canisters for used nuclear fuel may contribute to the occurrence of stress corrosion cracking. We demonstrate the use of fiber-optic laser-induced breakdown spectroscopy (FOLIBS) in the double-pulse (DP) configuration for high-sensitivity, remote measurement of the surface concentrations of chlorine compatible in constrained space and challenging environment characteristic for dry cask storage systems. Chlorine surface concentrations as low as 5 mg/m<sup>2</sup> have been detected and quantified by use of a laboratory-based and a fieldable DP FOLIBS setup with the calibration curve approach. The compact final optics assembly in the fieldable setup is interfaced via two 25-m long optical fibers for high-power laser pulse delivery and plasma emission collection and can be readily integrated into a multi-sensor robotic delivery system for *in-situ* inspection of dry cask storage systems.

© 2018 Elsevier B.V. All rights reserved.

## 1. Introduction

The extended usage of the dry cask storage systems (DCSS) that results from the delay in opening of a permanent geological repository for used nuclear fuel has raised serious concerns about the overall structural integrity of DCSS [1–3]. Remote inspection of DCSS that comprises a stainless steel canister and concrete overpack is desired, which motivates the development of a multi-sensor robotic inspection system for such purpose. One example of an effort that could lead to accurate and comprehensive inspections is development of the Portable Robotic Inspection of Nuclear Storage Enclosures (PRINSE) system [4]. Stress corrosion cracking (SCC) has been considered to be the most likely degradation mechanism of steel canisters at marine sites. The accumulation of chlorine (Cl) anions in the deliquescent airborne sea salt particles deposited on the heat affected zones of the welding lines over a long service life may provide sufficient Cl, as well as susceptible materials and tensile thermal stresses that are responsible for SCC [5,6]. According to a field

test conducted in Japan, the typical Cl concentration observed on the steel canister is in the range of 1–100 mg/m<sup>2</sup> [7]. Although the concentration may be significantly affected by the environmental conditions [6], we targeted this Cl surface concentration range in our study.

Laser-induced breakdown spectroscopy (LIBS) has proven to be an effective approach for detection of Cl attached to stainless steel surfaces [8,9]. However, the sensitivity of the Cl concentration measurement via LIBS is limited by the high ionization potential of Cl and by the difficulty in populating the relatively high upper level energy of neutral chlorine for the transition of interest. This is especially the case when high-power laser pulses need to be delivered by flexible fiber optics through the duct of the air ventilation system of DCSS. In this situation, the maximum laser irradiance that can be achieved at the sample surface is limited by multiple factors related to the optical fiber, including its aperture, laser coupling efficiency, optical damage threshold, intermodal dispersion, and the focusing conditions that can be practically realized post fiber exit. Fiber-optic laser-induced breakdown spectroscopy (FOLIBS), ever since its emergence, has been successfully applied to a number of “real-world” applications that require remote *in-situ* analysis; however, in none of them there was special attention paid to the halogen Cl,

\* Corresponding author at: Department of Nuclear Engineering and Radiological Sciences, University of Michigan, Ann Arbor, MI 48109, United States.  
E-mail address: [ijov@umich.edu](mailto:ijov@umich.edu) (I. Jovanovic).

which is difficult to detect through its optical emission [10–15]. In recent work, Eto and Fujii [9] demonstrated the potential to detect Cl emissions in FOLIBS at Cl surface concentrations of approximately 50 mg/m<sup>2</sup>. However, reliable detection of the most intense Cl I emission line (837.6 nm) under typical LIBS ablation conditions and located outside the vacuum ultraviolet region remains challenging when quantitative measurements of Cl on steel surfaces are sought at even lower concentrations. Efforts were undertaken to improve the sensitivity of Cl measurement by detecting alkali metals as surrogates for Cl [16]. However, this measurement could become inaccurate if Cl speciation occurred during the transport of salt in the environment, such that the ratio of concentrations of alkali metals to Cl could be modified [6]. Direct Cl measurement in FOLIBS is therefore motivated to a significant extent by the desire to overcome the limitations of the surrogate measurements. Special approaches, such as the use of helium buffer gas [17], additional excitation by electrical discharge [18], and double-pulse (DP) excitation technique [19], can be explored to improve the sensitivity and accuracy of direct Cl measurement in FOLIBS. From those approaches, the DP excitation technique appears most suitable for use in the DCSS environment.

DP excitation is expected to significantly enhance the characteristic emissions from the plasma through a reheating process by a second laser pulse, such that denser and hotter plasma can be formed, containing a large population of analyte atoms that are sufficiently excited to contribute to the desired Cl I 837.6 nm emission line [20]. Extensive laboratory studies of detection of Cl using DP LIBS have demonstrated the effect of the use of a second laser pulse by varying its wavelength, energy, and inter-pulse delay in orthogonal geometry [17,21]. Labutin *et al.* first explored the possibility of using DP technique in a more practical collinear configuration to assist the excitation of Cl atoms, and observed prominent enhancement of the analytical Cl I line at 837.6 nm using a DP approach in their laboratory study [19]. A limit of detection (LOD) for chlorine of 50 ppm in concrete was achieved by using an internal standard of the Mg II line at 279.08 nm. Additionally, a mobile system, equipped with an air-cooled Q-switched Nd:YAG laser (1064 nm), a compact Czerny-Turner spectrometer, and an ungated CCD camera was also developed by this group, achieving an LOD of 1500 ppm for Cl. The aim was *in-situ* quantification of corrosive active non-metals under ambient conditions in concrete, and represents a promising way for probing for presence of Cl in the field [22]. It should be noted that none of these prior studies incorporated optical fibers for high-power laser pulse delivery, such as in FOLIBS. Another obvious advantage of using DP in FOLIBS is simply that more energy can be delivered onto the target when splitting a single pulse into two separate pulses that are delayed with respect to each other while propagating through the optical fiber.

In this study, a collinear DP configuration was adopted in FOLIBS to enable the observation of the Cl I emission line at 837.6 nm on the steel surface under ambient conditions, with a goal to achieve sensitivity to lower Cl concentrations. Two DP FOLIBS setups have been developed and tested. The first setup enables the study of the feasibility of DP FOLIBS for direct Cl detection in laboratory conditions, while the second has been designed to be more compact, aiming to fulfill the practical requirements of the remote inspection of DCSS. Standard samples for conventional LIBS calibration curve approach were prepared on steel substrates using a nebulizer-based process developed for our prior surrogate measurements [16]. No aggregation and crystallization of salt aerosols was observed on the sample surfaces with scanning electron microscopy (SEM). The surface concentration of Cl on the prepared samples is in the range of 1–100 mg/m<sup>2</sup>, calculated on the basis of deposition parameters and further confirmed by ion chromatography (IC). It is demonstrated in this study that the DP FOLIBS approach, which is fully compatible with integration into a robotic delivery system such as PRINSE [4,23], can detect Cl on stainless steel surfaces with sufficiently high sensitivity to meet the most demanding targets of DCSS inspection.

## 2. Experimental setup and methods

### 2.1. Sample preparation

To benchmark the LIBS measurement, the standard samples were prepared through the use of PerkinElmer Mira-mist nebulizer (P/N N0775330), which produces a fine mist when delivering the synthetic seawater solution (ASTM D1141-98, Lake Products Company LLC), which interacts with an argon gas stream. The volumetric flow rate of the nebulizer was calibrated to be 0.25 mL/min, and the diameter of the spraying area was measured to be 4.5 cm when the nebulizer was kept 15 cm above the substrate. The stainless steel substrates were preheated by a Thermo Scientific Cimarec hot plate to 500 °C to provide near-instantaneous vaporization of water on contact with the heated surfaces, and helped avoid the aggregation of aerosol particles and formation of salt crystals, as can be seen under SEM measurement in our previous work [16]. This resulted in more homogeneous salt deposition relative to the unheated case. In order to prevent significant cooling down of the substrates during spraying, the selected dilution factor of 1/100 limited the exposure time of the substrates to less than 1 min. The Cl surface concentrations of the samples were calculated from the mass concentration of Cl in the diluted seawater solution, the flow rate of the nebulizer, the exposure time of the samples, and the sprayed area. The absolute surface concentrations of Cl on samples were further validated by IC (ICS 2500, Dionex Corp.), which is able to quantify Cl anions down to ~20 ppb when the salt depositions were washed off from the sample surfaces and dissolved in deionized water.

### 2.2. Laboratory DP FOLIBS setup

In the laboratory DP FOLIBS setup shown in Fig. 1, a Q-switched Nd:YAG laser (Quanta-Ray PRO-250-10, Spectra Physics) with pulse duration of ~10 ns and a repetition rate of 10 Hz was operated at its fundamental wavelength of 1064 nm. The beam diameter was first reduced using a Galilean telescope, and then the pulse was split using a plate beamsplitter. With this configuration, the path of one of the resulting pulses was increased by 12 m with respect to the other path, resulting in an inter-pulse delay of 40 ns, when the pulses were recombined by means of two half-wave plates and a polarizing beamsplitter. A similar DP scheme is commonly seen in femtosecond DP LIBS [24,25], in which the maximum enhancement effect is usually found when the inter-pulse delay is on the order of picoseconds [20,26]. However, the physical processes involved in the nanosecond laser-material interaction are known to differ significantly from those that occur when nanosecond lasers are used, such that the timescale of the plasma evolution may be very different [26]. Despite the fact that an inter-pulse delay on the order of magnitude of microseconds generally yields the strongest plasma enhancement in nanosecond DP LIBS [20,26], it is not practical to split a single laser pulse and provide the required hundreds of meters of optical delay for one of the pulses.

The DP sequence was coupled into the 10-m long optical fiber (Thorlabs FT1000EMT, 1-mm core diameter, NA = 0.39) using a plano-convex lens with a focal length of 300 mm. The input end face of the fiber was positioned slightly beyond the focus of the 300-mm lens to prevent fiber damage. Despite the lower coupling efficiency to the sample during ablation with the single pulse [27], the usage of IR wavelengths in DP configuration provided: (i) lower probability of damaging the fiber using 1.17 eV (1064 nm, fundamental wavelength of the Nd:YAG laser) photons compared to higher harmonics, such as 532 nm (second harmonic of the Nd:YAG laser); (ii) greater overall energy throughput; and (iii) strong plasma absorption of the second pulse, leading to enhancement of emission signal.

Two tight-focusing plano-convex lenses (30 mm focal length) were used to collimate the highly divergent DP sequence focal from the

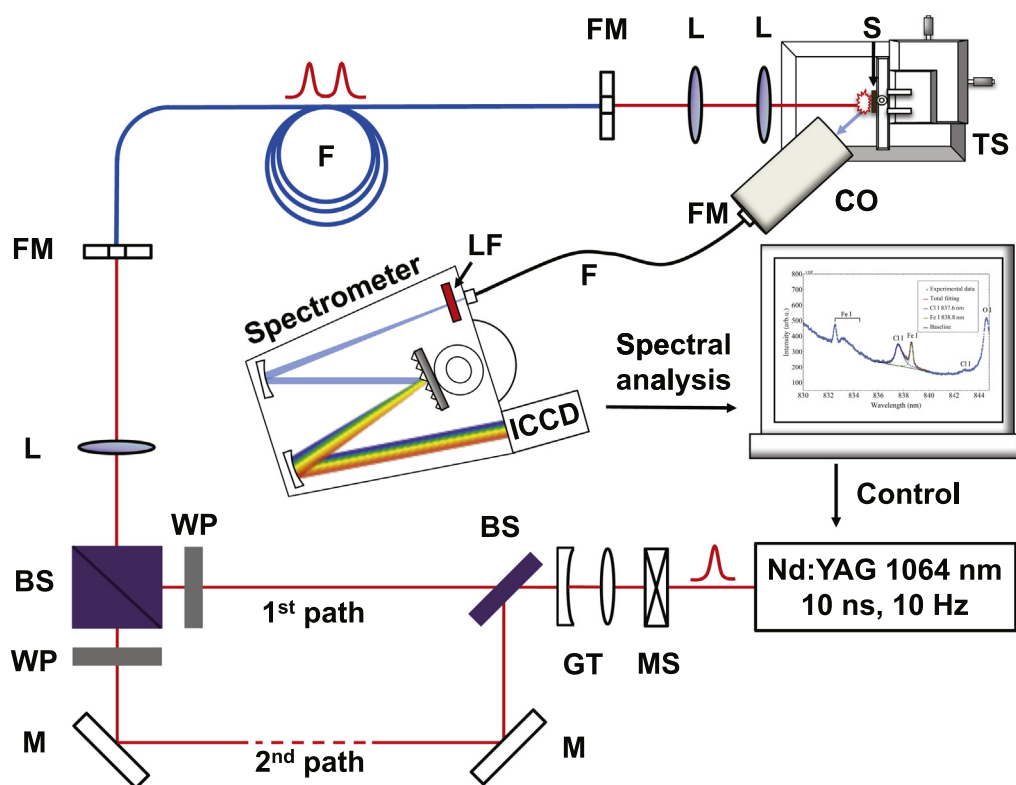


**Fig. 1.** Laboratory experimental setup for DP FOLIBS measurement (BS: beamsplitter, CO: collection optics, F: fiber, FM: fiber mount, GT: Galilean telescope, L: lens, LF: long-pass filter, M: mirror, MS: mechanical shutter, S: sample, TS: translation stage, WP: wave plate).

fiber and focus the pulses onto the sample surfaces to form the plasma. The plasma emission was collected by a 50-mm plano-convex lens positioned at  $45^\circ$  with respect to the incident beam and transported by a separate 400- $\mu\text{m}$  diameter quartz fiber to the Czerny-Turner spectrometer (iHR550, Horiba Jobin Yvon) with 1200-grooves/mm diffraction grating. The spectrometer system was calibrated using a deuterium-halogen light source (DH-2000, Ocean Optics). A long-pass filter with a cutoff wavelength at 550 nm was placed behind the entrance of the spectrometer to eliminate the second-order diffraction of the iron lines in the region near 400 nm. The Andor iStar 334T intensified charge-coupled device (ICCD) supported the time-gated detection in LIBS, whereas the delay generator (DG645, Stanford Research Systems) provided proper timing between the mechanical shutter and the gating of the ICCD camera. The gating and timing is fully controlled by the Solis S acquisition software from Andor. A 3-axis travel translation stage provided precise motion control of the sample and allowed exposing of “fresh” points on the surface of sample manually when performing surface averaging.

### 2.3. Fieldable DP FOLIBS setup

The fieldable DP FOLIBS setup has been designed to meet the space constraints of the PRINSE system and to allow rapid *in-situ* analysis. This experimental arrangement consists of a Q-switched Nd:YAG laser (Evergreen 70, Quantel) that houses two collinearly combined laser heads, allowing a continuously adjustable interpulse delay. The DP laser operated at  $\sim 60$  mJ per pulse with a pulse duration of  $\sim 15$  ns and a repetition rate of 10 Hz. As shown in Fig. 2 (a), the fiber coupling of the DP sequence is achieved using a 200-mm focal length lens. In order to accommodate the requirements for field deployment, the lengths of the optical fibers used for laser delivery

and spectral measurement were both extended to 25 m. The top view of the design of the remote optical assembly is shown in Fig. 2 (b); this assembly [23] can be fit into and be carried by the robotic delivery cars for inspection of DCSS. In the design, the DP (represented by a red beam) is collimated by the fiber collimator (F810SMA-1064, Thorlabs) and focused using a 24.5-mm plano-convex lens. A mirror diverts the converging beam vertically to the sample surface. During LIBS measurements, this last mirror requires regular cleaning due to the deposition of microparticles produced in laser ablation. The parabolic mirror views the plasma from a  $60^\circ$  angle with respect to the incident laser beam. The collimated plasma emission (represented by a blue beam) is coupled into the fiber by a 30-mm plano-convex lens. A LabVIEW [28]-based system provided timing control of both laser pulses and the ICCD gate through the ICCD's internal digital delay generator. For the purpose of characterizing the optics assembly in the lab environment, an automated 3-axis linear stage allowed for efficient and repeatable scanning of the stainless-steel samples.

## 3. Results and discussion

### 3.1. Characterization of fiber optic transport

The laser power (and thus its energy) that can be transmitted through the fiber is constrained by optical damage to the fiber. Multimode fibers with large core diameters can transmit higher peak powers, but offer only limited focusability upon propagation through the fiber. The minimum focal spot size that can be obtained following the laser transport through such fiber increases linearly with its core diameter. We found experimentally that sufficient laser irradiance can be obtained to observe the 837.6-nm Cl I emission line even at low Cl concentrations, well below  $100 \text{ mg/m}^2$ .

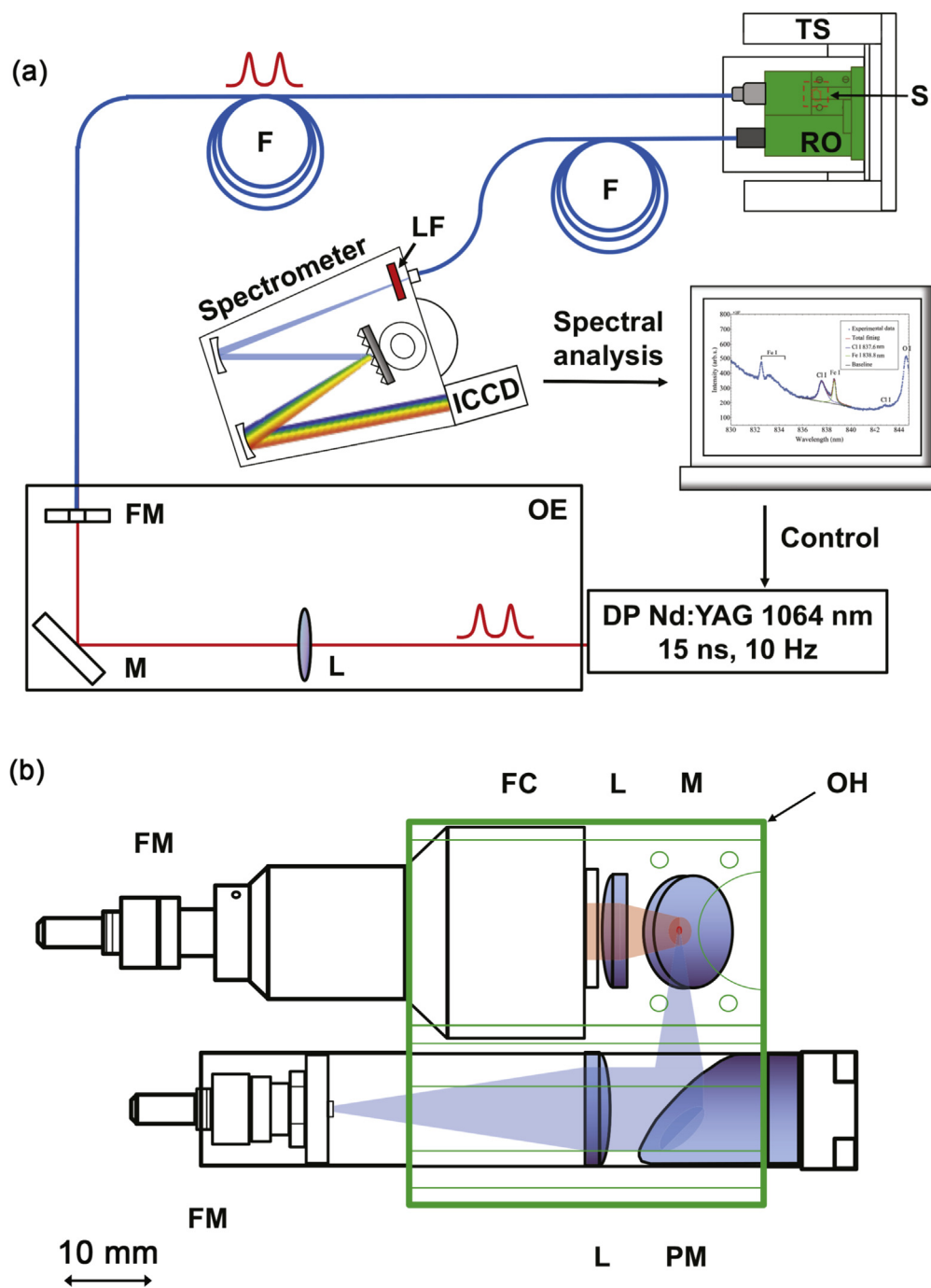


**Fig. 2.** (a) Experimental setup for fieldable DP FOLIBS measurement (F: fiber, FC: fiber collimator, FM: fiber mount, L: lens, LF: long-pass filter, M: mirror, OH: optics holder, PM: parabolic mirror, RO: remote optics, S: sample, SP: spectrometer, TS: translation stage); (b) Top view of remote optics design for robotic delivery car in fieldable DP FOLIBS system. (For interpretation of the references to color in this figure, the reader is referred to the web version of this article.)

Fig. 3 shows the energy transmission efficiency of the multimode fiber used for laser pulse delivery. The minimum angular curvature during experiments was 35.4 rad/m. A maximum total input energy of 81 mJ was achieved for the DP sequence obtained in the laboratory setup. However, damage was frequently observed at a depth of approximately 10 mm from the fiber surface, which prevented continuous operation at the upper limit of the input pulse energy. This phenomenon may be caused by the first internal reflection of the laser beam inside the fiber [29]. To confirm that proper alignment was achieved for both DP laser paths, we also recorded the output energy from a single-pulse (SP) input by blocking either

of the DP laser paths. Linear regression of both SP and DP experiments shows that the transmission efficiency was approximately 66%. A R-squared value of 0.99 obtained demonstrates both the absence of significant nonlinear effects and a high stability in coupling of laser pulses to the fiber, since each of the data points was collected in a different experiment over a period of time. In the fieldable setup, the maximum total input energy was significantly increased due to much higher beam quality provided by the DP laser and the use of a longer laser pulse width. The transmission efficiency of the fiber started to degrade at approximately 120 mJ per DP sequence.

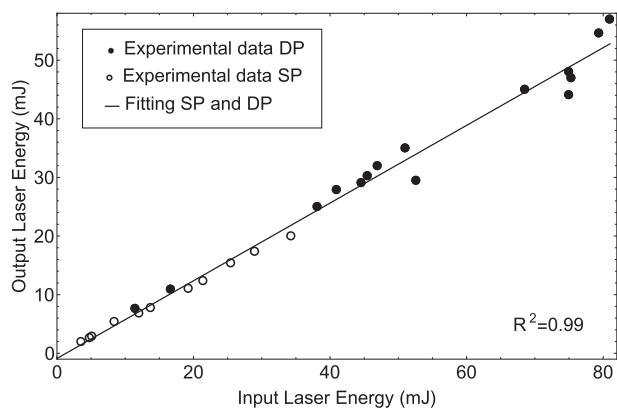


**Fig. 3.** Energy transmission efficiency of the step-index 1-mm core diameter multimode fiber (Thorlabs FT1000EMT). The solid line is the linear regression of the experimental data in both SP (open circle) and DP (solid circle). The SP data was obtained by blocking either of the laser paths between the beamsplitters in the laboratory setup.

As the length of the fiber is extended to 25 m in the fieldable setup, the broadening of the laser pulses when propagating through the fiber should be considered. The group delay due to the intermodal dispersion in the fiber at the critical angle is given by:

$$T_g = \frac{n_1 L (n_1 - n_2)}{c n_2}, \quad (1)$$

where  $L$  is the fiber length,  $c$  is the speed of light, and  $n_1$  and  $n_2$  are the refractive indices of the fiber core and cladding material, respectively. Referring to the specifications of the multimode fiber provided by the manufacturer, a 4.79-ns intermodal dispersion can be obtained, while the material dispersion in the fiber is only on the order of picoseconds. As a result, the pulse duration at the output of the multimode fiber is

$$\tau_2 = (\tau_1^2 + \tau_i^2)^{1/2}, \quad (2)$$

where  $\tau_1$  is the pulse duration before propagation through the fiber and  $\tau_i$  is the intermodal dispersion of the multimode fiber. A 0.85-ns broadening can be calculated for the input 15-ns laser pulse, resulting in an output pulse duration of 15.85 ns, which is in good agreement with the 16.1-ns pulse measured at the fiber output and shown in Fig. 4. No significant effect due to this broadening was observed in our experiments.

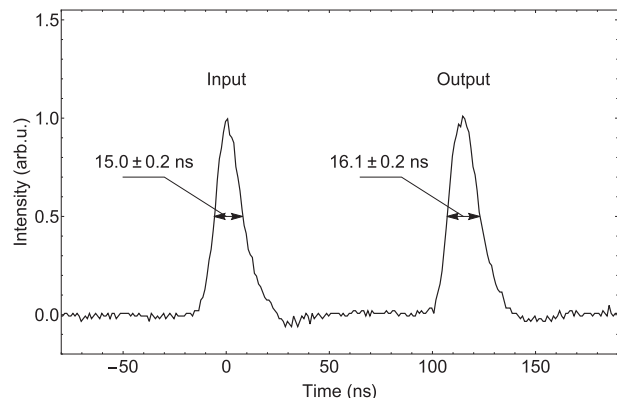


**Fig. 4.** Pulse duration measured before and after the 25-m long multimode fiber.

Fig. 5 (a) and (b) shows the SEM images of the laser spots on the stainless steel substrates in both SP and DP ablations in the laboratory setup. A speckle pattern with a characteristic diameter of  $\sim 600 \mu\text{m}$  can be observed due to the interference among the myriad guided modes in the fiber. The full overlap of the two laser pulses achieved by coupling into a single fiber shows its advantage over the setup that adopted separate fibers for delivery of each laser pulse in a single DP sequence, which resulted in partial overlap of the beam spots [30]. It is known that when a DP approach is used, a greater fraction of the incident laser energy is deposited directly into the preformed plasma rather than onto the underlying material [31]. Consistent with this feature of the DP approach, we observe no surface structure, such as the large thermally affected area seen in earlier observations with open beam delivery [16], and which results from the high thermal gradient in the vicinity of the focal spot.

### 3.2. Spectral analysis for quantification of Cl concentration on stainless steel

#### 3.2.1. Laboratory DP FOLIBS setup

Plasma reheating by the second laser pulse in DP can increase the plasma temperature and facilitate the electron impact excitation reactions in the ablated material. Additionally, DP technique can enhance the material removal, improve atomization, and increase the plasma volume. These mechanisms are reported to contribute to the enhancement of the characteristic emission from excited atoms [20]. More importantly, by using the DP approach, twice the laser energy can be delivered through the optical fiber when compared to the SP, limited by optical damage. The enhancement effect of DP excitation in FOLIBS can be clearly observed through direct comparison of SP and DP spectra of 100-mg/m<sup>2</sup> sample obtained in the laboratory setup, as shown in Fig. 6. Approximately a five-fold increase of the emission lines was achieved by use of DP technique relative to SP, which allows the detection of Cl at much lower concentrations. It should be noted that, in both SP and DP schemes, the FOLIBS systems operated approaching maximum power capacity.

To develop the calibration curve of the Cl I line at 837.6 nm in the laboratory DP FOLIBS setup, emission spectra in the spectral range of 830–844.8 nm were recorded and are shown in Fig. 7 (a). The reported spectra represent an average of the emission measured at five different locations near the center of the standard sample, with a single DP sequence at each location. Considering the much larger Einstein coefficient of Cl relative to Fe, a short ICCD gate delay of 0.1  $\mu\text{s}$  was adopted. The gate delay was optimized by maximizing the Cl emission while suppressing the relative emission intensity of Fe to Cl for better resolving the Cl line at 837.6 nm from the interfering intense Fe line at 838.8 nm. A long gate width of 15  $\mu\text{s}$  was used to enhance the collection of Cl emission. The CCD gain was set to be 1000 during experiments. The DP laser energies at the input and output of the fiber were 75 mJ and 45 mJ, respectively, whereas approximately 39 mJ was delivered onto the sample surface due to the coupling loss of the collimating lens that is insufficient to fully cover the diverged output beam. In the spectra, the Cl I line at 837.6 nm from the multiplet of  $4^4D^0 \rightarrow 4^4P$  has the highest intensity, and the neighboring intense emission of Fe I at 838.8 nm is also present. Shadowed by the intense Fe I group around 832–835 nm and the O I line at 842.8 nm, the other two Cl I lines at 833.3 nm and 842.8 nm from the Cl multiplet can be observed only at higher Cl concentrations.

An increase and broadening of the 837.6-nm Cl I line can be observed with the increase of Cl concentration from 5 mg/m<sup>2</sup> to 100 mg/m<sup>2</sup>. Although the Fe I lines and the O I line show variations between different Cl concentration levels due to plasma fluctuation originating from complex laser-material interaction, they do not show such a strong increasing trend with the increase of Cl concentration. Due to the long gate width used, the Cl line shows an asymmetric profile that is strongly influenced by the Stark effect.

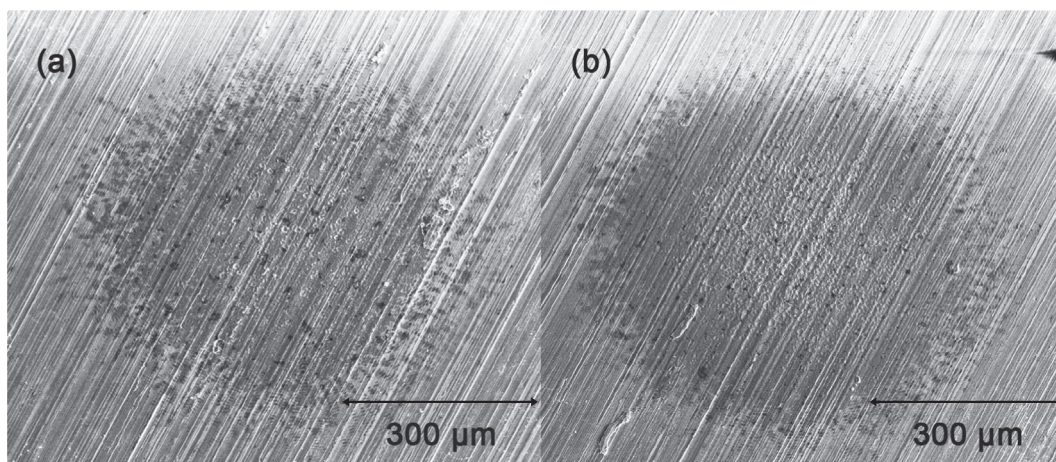


Fig. 5. SEM image (FESEM: NanoSEM630) of the laser ablation spots: (a) SP in laboratory setup; (b) DP in laboratory setup.

Multiple peak fitting with pseudo-Voigt distributions were used for spectral analysis to account for the spectral line intensity (area under the curve above background). An approach using a sigmoidally varied line width [32] was adopted to analyze the asymmetric profile of Cl peak. The nonlinear least-squares fitting was conducted using the Levenberg-Marquardt algorithm provided in the Mathematica framework [33]. The peak area of the Cl I line and its neighboring Fe I line were used for quantification, where the Fe I line serves as an internal standard to account for the possible effect of plasma fluctuation.

Fig. 7 (b) shows the dependence of relative peak area intensity of the Cl I line at 837.6 nm to the Fe I line at 838.8 nm on calculated Cl concentration in the range of 5–100 mg/m<sup>2</sup>. The mean value of the relative peak area intensity was fitted using a linear model. Standard deviation of relative peak area intensity is shown as vertical error bars, while the displayed horizontal ones are the result of an approximate 3 s timing uncertainty in sample preparation process. Uncertainty that originates from the Gaussian-shaped spraying distribution of the nebulizer is not included. The coefficient of determination of the linear fitting was found to be 0.91, which shows noticeable improvement from that of 0.87 determined by using unnormalized signal, suggesting that DP excitation technique with the use of Fe line as internal standard can improve the sensitivity of FOLIBS and allow direct Cl measurement on steel surfaces to as low as 10 mg/m<sup>2</sup>. Another commonly used normalization method incorporating rationing of the peak areas to the total plasma

emission intensity [34] do not show comparable performance as the internal standardization currently used in the work. It should be noted that the fixed inter-pulse delay of 40 ns in the laboratory setup precludes the maximization of the enhancement of the line intensity that the DP approach offers [20]. The use of a DP laser with adjustable

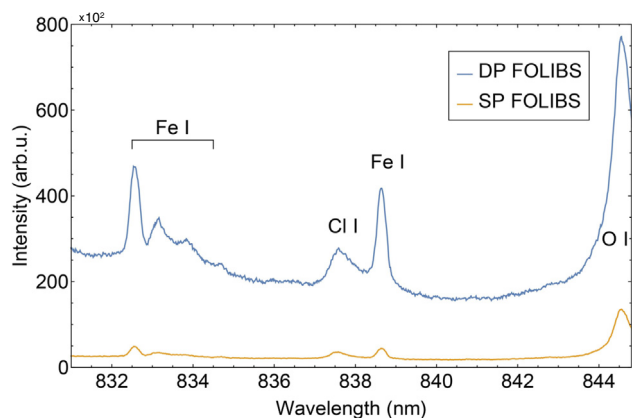


Fig. 6. Emission spectra of 100-mg/m<sup>2</sup> sample near the Cl I 837.6 nm line obtained using SP and DP excitation in the laboratory FOLIBS setup.

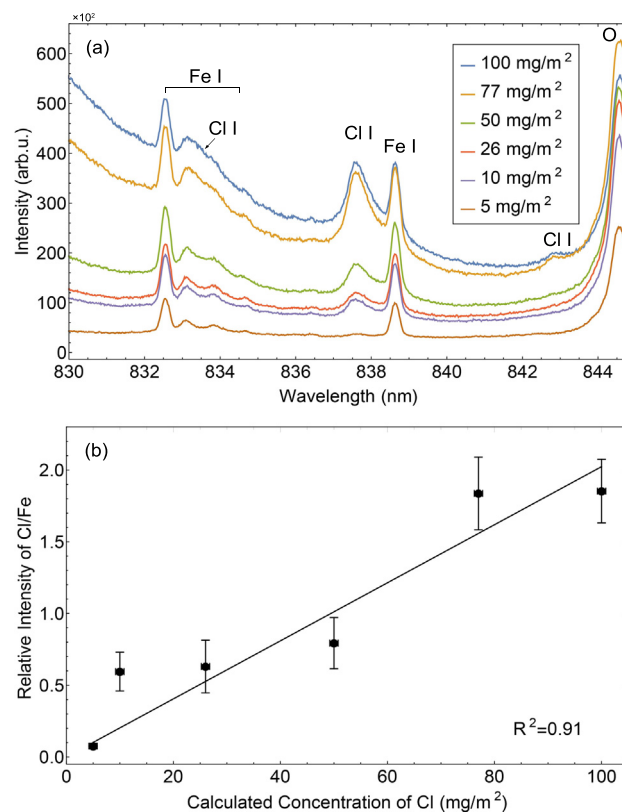


Fig. 7. (a) Emission spectra averaged over positions of Cl I multiplet obtained from samples with Cl concentration in the range of 5–100 mg/m<sup>2</sup> in the laboratory FOLIBS setup. The delivered DP laser energy onto the sample surface was 39 mJ. The gate delay, gate width, and gain of the ICCD camera were 0.1 μs, 15 μs, and 1000, respectively; (b) dependence of the relative emission intensity (peak area) of Cl I (837.6 nm) to Fe I line (838.8 nm) on the calculated Cl concentration in the range of 5–100 mg/m<sup>2</sup>. The solid line is the linear regression of the experimental data (solid circle). The vertical error bars represent the standard deviation of the emission intensities at five different positions. The horizontal error bars originate only from 3-s timing uncertainty in the sample preparation process.

inter-pulse delay in the fieldable setup can improve the analytical performance of FOLIBS through optimized laser-plasma coupling.

### 3.2.2. Fieldable DP FOLIBS setup

Enhancement effect is observed at different time scales depending on the characteristics of plasma formed by the laser ablation process. Parametric study of the optimum conditions for maximizing the Cl I emission intensity at 837.6 nm was conducted prior to the development of a calibration curve for direct Cl measurement in the fieldable FOLIBS setup. Automatic surface scanning with a raster step size of 1 mm was performed in fieldable DP FOLIBS setup. A total  $25 \times 25$  sampling points were used over the sample surface. The peak area intensity of the Cl I line was analyzed using a custom LabVIEW program, developed specifically for real-time, batch processing analysis of spectra for on-site DCSS inspection. A pseudo-Voigt peak shape with a polynomial baseline was used in the multiple peak fitting within the selected spectral range. The Levenberg-Marquardt algorithm was provided by the LabVIEW Nonlinear Curve Fit VI. In the parametric study, two parameters – the inter-pulse delay of the DP laser sequence and the time delay of the gate of the ICCD – were varied, while keeping the gate width and gain of the ICCD fixed.

Fig. 8 shows the contour plot of the peak area intensity of the Cl I line at 837.6 nm obtained from a 50-mg/m<sup>2</sup> standard sample. The inter-pulse delay was varied between 800 ns and 1200 ns with a step size of 100 ns, whereas the gate delay was varied between 300 ns and 2700 ns with a step size of 300 ns. The gate width and the gain of the ICCD were 300 ns and 2500, respectively. The Cl I intensity for each set of parameters was averaged over fourteen randomized locations using the programmable sampling. Three DP acquisitions at each location were performed. The resulting contour map, which has been linearly interpolated, indicates the regions in which the LIBS signal is maximized at a Cl concentration of 50 mg/m<sup>2</sup>, suggesting a 900-ns inter-pulse delay and a 600-ns gate delay exhibit the greatest enhancement of Cl emission. Therefore, we adopted an inter-pulse delay of 900 ns for developing the calibration curve in our fieldable FOLIBS setup through analyzing the spectra integrated from a gate delay of 300 ns to 2100 ns. To avoid severe Stark effect experienced in the laboratory setup, the gate width was reduced significantly. However, due to the limited field of view provided by the compact remote optics, a relatively long 1.9 μs gate width was kept,

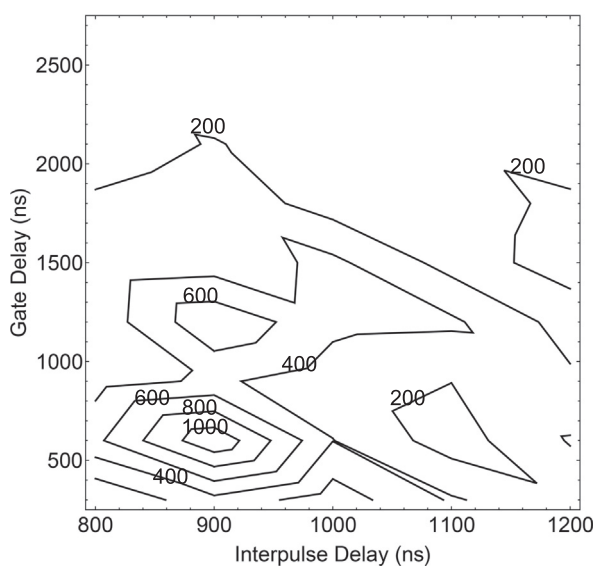


**Fig. 8.** Parametric contour map of the Cl I (837.6 nm) emission intensity (peak area) versus the inter-pulse delay and the gate delay obtained using a sample with Cl concentration of 50 mg/m<sup>2</sup>. The gate width and gain of the ICCD were set to 300 ns and 2500, respectively.

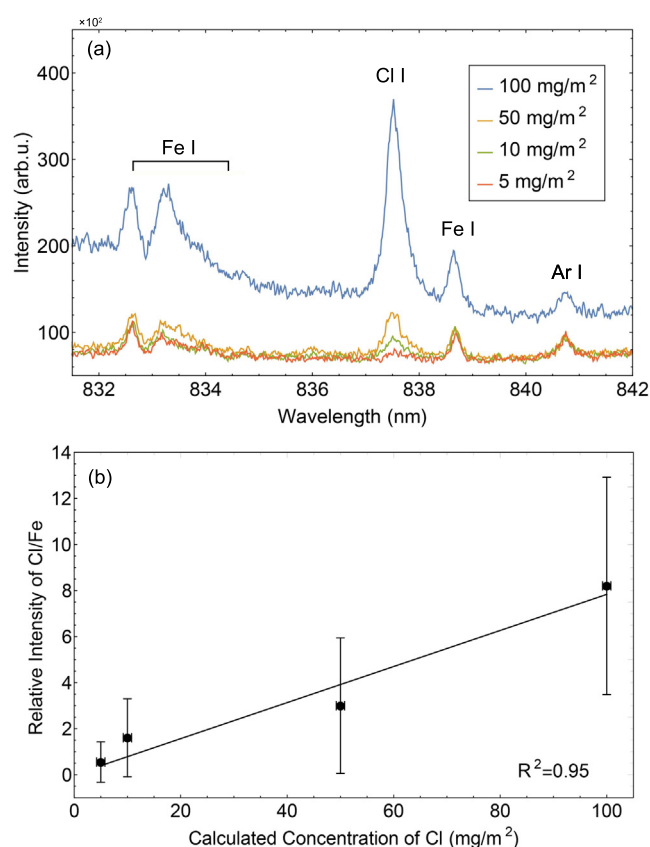


**Fig. 9.** (a) Emission spectrum of Cl I multiplet obtained from samples with Cl concentration in the range of 5–100 mg/m<sup>2</sup> in fieldable FOLIBS setup. The inter-pulse delay of the laser burst was set to 900 ns. The gate delay, gate width, and gain of the ICCD camera were set 300 ns, 2100 ns and 2500, respectively; (b) dependence of the relative emission intensity (peak area) of Cl I (837.6 nm) to Fe I (838.8 nm) on the calculated Cl concentration in the range of 10–100 mg/m<sup>2</sup>. The solid line is the linear regression of the experimental data (solid circle). The horizontal error bars originate only from 3-s timing uncertainty in the sample preparation process.

which results in a higher consistency of the plasma emission, while still maintaining a good signal-to-background ratio by keeping the inter-pulse delay at 900 ns. In previously reported work, the optimal value for inter-pulse delay was in the range of 1.5–4 μs [17,19,22], which may result from the differences in the laser wavelength, pulse energy, and matrix among these studies.

The emission spectra in the spectral range of 831.5–842 nm are shown in Fig. 9 (a), which represent an average of emissions from fourteen randomized locations on the sample surface with three DP samples taken at each location. The broadening of the Cl I line at 837.6 nm was less pronounced and the Cl to Fe intensity ratio was enhanced noticeably as compared to that obtained in the laboratory setup, which results in a better separation of the Cl I line from its neighboring Fe I line, and improves the accuracy of spectral analysis. Fig. 9 (b) shows the dependence of the relative peak area intensity of the Cl I line to its neighboring Fe I line on the calculated Cl concentration in the range of 5–100 mg/m<sup>2</sup>. The increased emission uncertainties shown in this calibration curve can be attributed to salt deposition profile that occurs due to the nature of sample preparation, in addition to plasma fluctuation. Fig. 10 shows the lateral distribution of emission intensity of the Cl I line obtained from a 10-mg/m<sup>2</sup> sample by  $25 \times 25$  automatic scanning over the entire sample surface. A well-defined deposition profile can be observed, which is consistent with the spraying pattern of the nebulizer. Although increasing the uncertainty, integrating over a surface area is more representative of the Cl surface concentrations that were

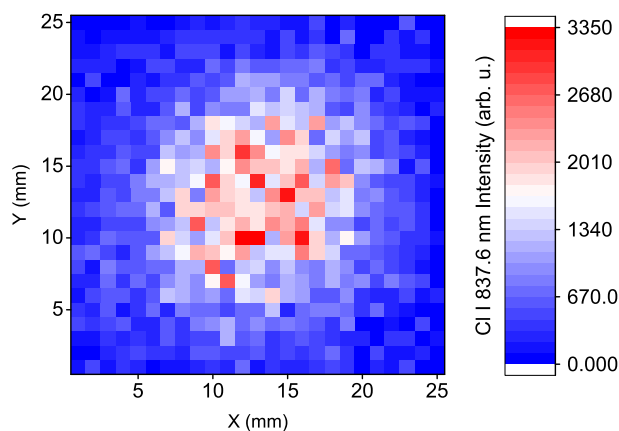


**Fig. 10.** Lateral distribution of the intensity of Cl I line at 837.6 nm obtained on a sample with Cl concentration of 10 mg/m<sup>2</sup>.

calculated assuming a uniform distribution in comparison to making measurements only near the center of the area where salt was deposited. A linear relationship between the Cl to Fe intensity ratio and the calculated Cl concentration was found with good correlation ( $R^2 = 0.95$ ), which indicates that direct Cl measurement in the fieldable FOLIBS system was achieved at the Cl concentration as low as 5 mg/m<sup>2</sup> with the assistance of DP excitation.

#### 4. Conclusion and perspective

In order to overcome the difficulties of direct Cl measurement on steel surfaces via FOLIBS, we explored the use of DP excitation technique to improve the analytical performance of LIBS in fiber delivery. When compared to a surrogate measurement, direct Cl measurement is a more reliable method for assessing the potential for SCC on steel canisters without the need to fully understand the transport and deposition of the sea salt aerosols on the surface. To the best of our knowledge, the DP excitation has allowed reliable quantification of Cl surface concentration on steel in the range of 5–100 mg/m<sup>2</sup> to be achieved via FOLIBS for the first time. Additionally, the potential for any detrimental effects to the material that could be induced by laser ablation is greatly reduced when the total delivered laser energy is split into two successive pulses in DP FOLIBS, so that less energy is deposited directly onto the sample surface when compared to single pulse delivery. The compact fieldable FOLIBS setup, which can be readily integrated into a multi-sensor PRINSE system, has been proven to be equally effective in direct Cl measurement on steel surfaces at a notably low limit of detection of 5 mg/m<sup>2</sup>.

The fieldable FOLIBS system has been tested in a mock-up of DCSS built at the Test Track facility of the Pennsylvania State University to demonstrate its capacity of *in-situ* measurement of Cl on steel canisters. For future work, the accuracy and the sensitivity of the FOLIBS system may be further improved through the refinement of the design of remote optics assembly by adopting a coaxial configuration in the focusing optical assembly [9], applying the mechanical spatial confinement of the plasma front propagation [35], or by providing fine adjustment to the optics in the upgraded assembly.

#### Acknowledgments

This work has been funded by the Department of Energy's Nuclear Energy University Program under Integrated Research Project award number DE-NE0008266. We thank the other members of our research group, especially C. Lissenden of Pennsylvania State University, for useful discussions and a fruitful collaboration.

#### References

- [1] O. Chopra, D. Diercks, R. Fabian, Z. Han, Y. Liu, Managing aging effects on dry cask storage systems for extended long-term storage and transportation of used fuel (REV. 2), Technical Report FCRD-UFD-2014-000476, Argonne National Laboratory (ANL), 2014.
- [2] R.M. Meyer, A.F. Pardini, J.M. Cuta, H.E. Adkins, A.M. Casella, H. Qiao, M.R. Larche, A.A. Diaz, S.R. Doctor, NDE to manage atmospheric SCC in canisters for dry storage of spent fuel: an assessment, Technical Report PNNL-22495, Pacific Northwest National Laboratory (PNNL), Richland, WA (United States), 2013.
- [3] D. Enos, C. Bryan, K. Norman, Data report on corrosion testing of stainless steel SNF storage canisters, Technical Report FCRD-UFD-2013-000324, US Department of Energy, Office of Used Nuclear Fuel Disposition, 2013.
- [4] C. Lissenden, S. Choi, H. Cho, A. Motta, K. Hartig, X. Xiao, S. Le Berre, S. Brennan, K. Reichard, R. Leary, et al. Toward robotic inspection of dry storage casks for spent nuclear fuel, *J. Press. Vessel. Technol.* 139 (2017) 031602.
- [5] S. Chu, Failure modes and effects analysis (FMEA) of welded stainless steel canisters for dry cask storage systems, Electric Power Research Institute Report 3002000815, 2013.
- [6] C.R. Bryan, D.G. Enos, SNF interim storage canister corrosion and surface environment investigations, Technical Report FCRD-UFD-2013-000324, Sandia National Laboratories (SNL-NM), Albuquerque, NM (United States), 2015.
- [7] M. Wataru, H. Kato, S. Kudo, N. Oshima, K. Wada, H. Narutaki, Measurement of atmospheric sea salt concentration in the dry storage facility of the spent nuclear fuel, Proceedings of 14th International Conference on Nuclear Engineering (ICONE), Miami, Florida, July 17–20, Paper No. ICONE14-89293, 2006, pp. 857–863.
- [8] S. Eto, J. Tani, K. Shirai, T. Fujii, Measurement of concentration of chlorine attached to a stainless-steel canister material using laser-induced breakdown spectroscopy, *Spectrochim. Acta B At. Spectrosc.* 87 (2013) 74–80.
- [9] S. Eto, T. Fujii, Laser-induced breakdown spectroscopy system for remote measurement of salt in a narrow gap, *Spectrochim. Acta B At. Spectrosc.* 116 (2016) 51–57.
- [10] C. Davies, H. Telle, D. Montgomery, R. Corbett, Quantitative analysis using remote laser-induced breakdown spectroscopy (LIBS), *Spectrochim. Acta B At. Spectrosc.* 50 (1995) 1059–1075.
- [11] D.A. Cremers, J. Barefield, A. Koskelo, Remote elemental analysis by laser-induced breakdown spectroscopy using a fiber-optic cable, *Appl. Spectrosc.* 49 (1995) 857–860.
- [12] R. Neuhauser, U. Panne, R. Niessner, Utilization of fiber optics for remote sensing by laser-induced plasma spectroscopy (LIPS), *Appl. Spectrosc.* 54 (2000) 923–927.
- [13] A.K. Rai, H. Zhang, F.Y. Yueh, J.P. Singh, A. Weisberg, Parametric study of a fiber-optic laser-induced breakdown spectroscopy probe for analysis of aluminum alloys, *Spectrochim. Acta B At. Spectrosc.* 56 (2001) 2371–2383.
- [14] A. Whitehouse, J. Young, I. Botheroyd, S. Lawson, C. Evans, J. Wright, Remote material analysis of nuclear power station steam generator tubes by laser-induced breakdown spectroscopy, *Spectrochim. Acta B At. Spectrosc.* 56 (2001) 821–830.
- [15] M. Saeki, A. Iwanade, C. Ito, I. Wakaida, B. Thornton, T. Sakka, H. Ohba, Development of a fiber-coupled laser-induced breakdown spectroscopy instrument for analysis of underwater debris in a nuclear reactor core, *J. Nucl. Sci. Technol.* 51 (2014) 930–938.
- [16] X. Xiao, S. Le Berre, K. Hartig, A. Motta, I. Jovanovic, Surrogate measurement of chlorine concentration on steel surfaces by alkali element detection via laser-induced breakdown spectroscopy, *Spectrochim. Acta B At. Spectrosc.* 130 (2017) 67–74.
- [17] K. Sugiyama, T. Fujii, T. Matsumura, Y. Shiogama, M. Yamaguchi, K. Nemoto, Detection of chlorine with concentration of 0.18 kg/m<sup>3</sup> in concrete by laser-induced breakdown spectroscopy, *Appl. Opt.* 49 (2010) C181–C190.
- [18] V. Burakov, V. Kiris, S. Raikov, Optimization of conditions for spectral determination of chlorine content in cement-based materials, *J. Appl. Spectrosc.* 74 (2007) 321–327.
- [19] T. Labutin, A. Popov, S. Raikov, S. Zaytsev, N. Labutina, N. Zorov, Determination of chlorine in concrete by laser-induced breakdown spectroscopy in air, *J. Appl. Spectrosc.* 80 (2013) 315–318.
- [20] V. Babushok, F. DeLucia, J. Gottfried, C. Munson, A. Miziolek, Double pulse laser ablation and plasma: laser induced breakdown spectroscopy signal enhancement, *Spectrochim. Acta B At. Spectrosc.* 61 (2006) 999–1014.
- [21] J. Pedarnig, M. Haslinger, M. Bodea, N. Huber, H. Wolfmeir, J. Heitz, Sensitive detection of chlorine in iron oxide by single pulse and dual pulse laser-induced breakdown spectroscopy, *Spectrochim. Acta B At. Spectrosc.* 101 (2014) 183–190.
- [22] T.A. Labutin, A.M. Popov, S.M. Zaytsev, N.B. Zorov, M.V. Belkov, V.V. Kiris, S.N. Raikov, Determination of chlorine, sulfur and carbon in reinforced concrete structures by double-pulse laser-induced breakdown spectroscopy, *Spectrochim. Acta B At. Spectrosc.* 99 (2014) 94–100.
- [23] D. Fobar, X. Xiao, M. Burger, S. Le Berre, A. Motta, I. Jovanovic, Robotic Delivery of Laser-Induced Breakdown Spectroscopy for Sensitive Chlorine Measurement in Dry Cask Storage Systems, 2018. (under review).
- [24] T. Somekawa, M. Otsuka, Y. Maeda, M. Fujita, Signal enhancement in femtosecond laser induced breakdown spectroscopy with a double-pulse configuration composed of two polarizers, *Jpn. J. Appl. Phys.* 55 (2016) 058002.
- [25] X. Zhao, Y.C. Shin, Laser-plasma interaction and plasma enhancement by ultrashort double-pulse ablation, *Appl. Phys. B* 120 (2015) 81–87.

- [26] A. Elhassan, A. Giakoumaki, D. Anglos, G. Ingo, L. Robbiola, M. Harith, Nanosecond and femtosecond laser induced breakdown spectroscopic analysis of bronze alloys, *Spectrochim. Acta B At. Spectrosc.* 63 (2008) 504–511.
- [27] M. Burger, D. Pantić, Z. Nikolić, S. Djaniže, Shielding effects in the laser-generated copper plasma under reduced pressures of He atmosphere, *J. Quant. Spectrosc. Radiat. Transf.* 170 (2016) 19–27.
- [28] National Instruments Corp., LabVIEW, Version 2016, Austin, TX.
- [29] S. Allison, G. Gillies, D. Magnuson, T. Pagano, Pulsed laser damage to optical fibers, *Appl. Opt.* 24 (1985) 3140–3145.
- [30] K.L. Eland, D.N. Stratis, J.C. Carter, S.M. Angel, Development of a dual-pulse fiber optic LIBS probe for in-situ elemental analyses, Proceedings of the International society for optics and photonics (SPIE), Boston, Massachusetts, September 19–22, Paper No. 3853, 1999, pp. 288–294.
- [31] G. Cristoforetti, G. Lorenzetti, P.A. Benedetti, E. Tognoni, S. Legnaioli, V. Palleschi, Effect of laser parameters on plasma shielding in single and double pulse configurations during the ablation of an aluminium target, *J. Phys. D. Appl. Phys.* 42 (2009) 225207.
- [32] A.L. Stancik, E.B. Brauns, A simple asymmetric lineshape for fitting infrared absorption spectra, *Vib. Spectrosc.* 47 (2008) 66–69.
- [33] Wolfram Research, Inc., Mathematica, Version 11.0, Champaign, IL.
- [34] D. Body, B. Chadwick, Optimization of the spectral data processing in a LIBS simultaneous elemental analysis system, *Spectrochim. Acta B At. Spectrosc.* 56 (2001) 725–736.
- [35] A.M. Popov, F. Colao, R. Fantoni, Enhancement of LIBS signal by spatially confining the laser-induced plasma, *J. Anal. At. Spectrom.* 24 (2009) 602–604.